JBIC (1997) 2:623–633

ORIGINAL ARTICLE

Keith R. Barnard · Robert W. Gable
Anthony G. Wedd

Dioxo-, oxothio- and dithio-tungsten(VI) and tungsten(V) complexes of the ligand *N,N′*-Dimethyl-*N,N′*-bis(2-mercaptophenyl)ethylenediamine

Received: 9 April 1997 / Accepted: 30 June 1997

Abstract Synthesis of complexes *cis,cis*-$W^{V}OXL$ (X = Cl, NCS), *cis,trans*-$W^{V}OXL$ (X = Cl, OPh, SPh) and *cis,trans*-$W^{VI}E_2L$ ($E_2 = O_2$, OS, S_2) of the title ligand LH_2 are reported. *cis,cis*-$W^{V}OCIL$ crystallises in space group $P2_1/c$ with $a = 13.6541(9)$ Å, $b = 7.1555(11)$ Å, $c = 18.198(2)$ Å, $\beta = 95.294(6)°$, $V = 1770.4(3)$ Å^3 and $Z = 4$ while the *cis,trans* isomer crystallises in space group $P2_1/n$ with $a = 10.361(3)$ Å, $b = 14.141(4)$ Å, $c = 12.213(5)$ Å, $\beta = 102.56(3)°$, $V = 1747(2)$ Å^3 and $Z = 4$. *cis,trans*-$W^{VI}S_2L$ crystallises in space group $P2_1/n$ with $a = 10.645(2)$ Å, $b = 13.929(2)$ Å, $c = 12.189(2)$ Å, $\beta = 103.14(2)°$, $V = 1760(1)$ Å^3 and $Z = 4$. A short $CH_3\cdots Cl$ distance of 3.067(7) Å and an acute OWCl angle of 94.1(2)° are seen in *cis,cis*-$W^{V}OClL$, which converts to the *cis,trans* form on heating in MeCN. The latter isomer features a $CH_3\cdots Cl$ distance of 3.38(2) Å and an OWCl angle of 105.1(8)°. Electrochemical and EPR data are reported. In particular, *cis,trans*-$W^{VI}E_2L$ may be reduced to $[W^{V}E_2L]^-$. EPR properties of these anions and those of complexes $W^{V}OXL$ are discussed in the context of W^{V} centres in tungsten enzymes.

Key words Oxotungsten complexes · Tungsten enzymes

Abbreviations *acacH* acetylacetone · $bdtH_2$ 1,2-benzenedithiol · *Cys* cysteine · *d* diameter · $edtH_2$ 1,2-ethanedithiol · *EI-MS* electron impact mass spectrum · *EPR* electron paramagnetic resonance · *EXAFS* extended X-ray absorption fine structure · *Fc* ferrocene · *h* hour · LH_2 *N,N′*-dimethyl-*N,N′*-bis(2-mercaptophenyl)ethylenediamine · $L\text{-}N_3$ hydrotris(3,5-dimethylpyrazol-1-yl)borate anion · *n* number of electrons transferred · *SCE* saturated calomel electrode · *thf* tetrahydrofuran · *X* monanionic ligand.

K. R. Barnard · R. W. Gable · A. G. Wedd (✉)
School of Chemistry, University of Melbourne,
Parkville, Victoria 3052, Australia
e-mail: t.wedd@chemistry.unimelb.edu.au

Supplementary material Complete tables of crystallographic data, positional and thermal parameters, bond distances and angles (27 pages) plus observed and calculated structure factors (31 pages) are available from author A.G.W.

Introduction

A biochemistry of tungsten has emerged recently and undergone rapid development [1]. It is a feature of thermophilic organisms found in hot marine sediments and hydrothermal vents where the thermodynamic and kinetic properties of tungsten-pterin centres appear to favour their evolution over those of molybdenum [1–4]. The known tungsten enzymes play key roles in the assimilation of carbon from sources such as carbon dioxide, complex carbohydrates or proteins. The specific redox couples involved have very low potentials (≤ -400 mV versus the standard hydrogen electrode).

A crystal structure of the aldehyde oxidoreductase of *Pyrococcus furiosus* has revealed a square pyramidal tungsten centre bound to two 1,2-dithiolate bidentate ligands provided by a pterin cofactor (Fig. 1) [5, 6]. It was not possible to identify positively the other ligands in the crystallised form. Chemical and EXAFS studies of active forms are consistent with the presence of W = O, W = S and/or W-SH functions [1, 5, 7]. A second class of enzymes, exemplified by tungsten formate dehydrogenase, would appear to feature cysteine or selenocysteine in addition to the two 1,2-dithiolate bidentate ligands [1, 8]. These enzymes may be structurally similar to the molybdenum formate dehydrogenase enzyme whose crystal structure was reported recently [9]. A hydroxo rather than an oxo ligand is proposed for the Mo(VI) state. Despite these fascinating insights, the detailed nature of the active sites in the tungsten enzymes remains to be defined. The presence of oxo, hydroxo, thio, mercapto, thiolato, selenolato and O- and N-donor ligands are all possible. The chemistry is expected to involve tungsten in oxidation states IV–VI as these dominate established compounds bearing the above ligands.

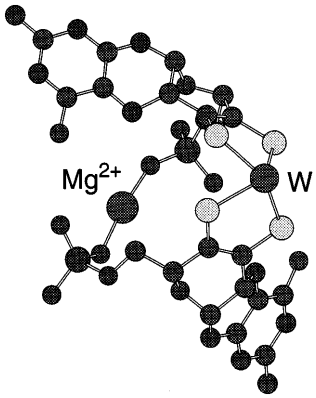

Fig. 1 Aldehyde oxidoreductase from *Pyrococcus furiosus* (resolution 2.3 Å): the tungsten atom is coordinated to two pterin 1,2-dithiolate ligands whose sulfur atoms lie in an approximate square plane [6]. Two other non-protein ligands may be present to complete a distorted trigonal prismatic site. The phosphate groups from each pterin cofactor bind to a six-coordinate Mg^{2+} ion

The $W^{VI}O_2$ group is relatively unreactive, and nature may use sulfur and/or selenium ligands to enhance the oxidative capacity of tungsten centers [1, 3]. Complexes $W^{VI}OSX(L\text{-}N_3)$ and $W^{VI}S_2X(L\text{-}N_3)$ featuring the tridentate ligand L-N_3 = hydrotris(3,5-dimethylpyrazol-1-yl)borate anion and monodentate anions X have been isolated and their chemistry explored [10, 11]. Interconversion of bis(ene-1,2-dithiolate) complexes of $W^{VI}O_2$, $W^{IV}O$ and $W^{VI}O(\eta^2\text{-}S_2)$ centres coupled to enzymatically relevant reactions, such as the oxidation of aldehydes to carboxylic acids, has been demonstrated [12, 13].

The present paper reports isolation and characterisation of W(VI) and W(V) complexes of the ligand LH_2 (Structure I). *Cis,cis* and *cis,trans* isomeric forms of $W^{V}OXL$ (X = monoanion) are described as well as *cis,trans*-$W^{VI}E_2L$ ($E_2 = O_2$, OS, S_2). The latter may be reduced to $[W^{V}E_2L]^-$ anions.

Experimental section

Materials

Synthesis of tungsten compounds was performed using standard Schlenk techniques under purified dinitrogen. Reagent grade solvents were dried and fractionally distilled under dinitrogen. Microanalyses were performed by either the Analytische Laboratorien, Elbach, Germany or Atlantic Microlabs Inc., Norcross, Georgia, USA.

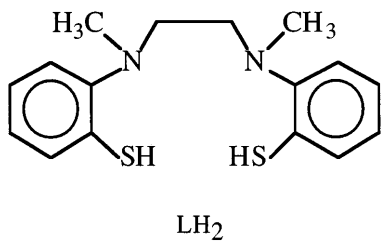

LH_2

Structure 1 Ligand LH_2

The ligand LH_2 [14, 15], *cis*-$W^{VI}O_2(acac)_2$ [16], and $(pyH)_2[W^{V}OCl_5]$ [17] were synthesised by literature methods. NaOPh was prepared by the reaction of NaOH with phenol [18], while NaSPh was prepared similarly from NaOH and freshly distilled thiophenol.

cis,trans-WO_2L

A solution of LH_2 (0.92 g, 3.0 mmol) in CH_2Cl_2 (5 cm^3) was added dropwise to a stirred suspension of *cis*-$WO_2(acac)_2$ (1.20 g, 2.90 mmol) in MeOH (70 cm^3). After 3 h, the fluffy yellow precipitate was filtered off in air, washed with MeOH and dried under vacuum. A second crop was obtained by refluxing the filtrate for 4 h. Recrystallisation from a CH_2Cl_2:Et_2O (1:1) solution afforded a yellow, microcrystalline product which was washed with Et_2O and dried under vacuum (0.98 g, 66%). Anal. Calcd for $C_{16}H_{18}N_2O_2S_2W$: C 37.1, H 3.5, N 5.4. Found: C 37.0, H 3.5, N 5.3. EI-MS: *m/z* 518. ^{1}H NMR ($CDCl_3$) 7.33–7.40 (m, Ph, 4 protons), 7.10–7.26 (m, Ph, 4), 3.78 (s, CH_3, 6), 3.35 (d, 10.5 Hz, CH_2, 2), 3.12 ppm (d, 10.4 Hz, CH_2, 2).

cis,trans-WS_2L

A suspension of B_2S_3 (0.53 g, 4.5 mmol) and *cis,trans*-WO_2L (0.28 g, 0.55 mmol) in benzene (20 cm^3) was refluxed for 21 h and the solvent removed under vacuum. Soxhlet extraction using CH_2Cl_2 (60 cm^3) afforded an orange solution which was reduced to 15 cm^3. Precipitated product was filtered off and redissolved in CH_2Cl_2 (15 cm^3). This solution and the original filtrate were applied separately to silica gel 60 columns (mesh 70–230, 37 cm × 1.8 cm diameter) in air. Upon elution with CH_2Cl_2 (10 cm^3 min^{-1}), the first (orange) bands were collected, concentrated and layered with *n*-hexane. Dark red rhombic crystals were washed with *n*-hexane and dried under vacuum (0.025 g, 8%). Anal. Calcd for $C_{16}H_{18}N_2S_4W$: C 34.9, H 3.3, N 5.1, S 23.3. Found: C 34.8, H 3.3, N 5.1, S 23.2. EI-MS: *m/z* 550. ^{1}H NMR ($CDCl_3$): 7.1–7.4 (m, Ph, 8), 3.82 (s, CH_3, 6), 3.22 (m, CH_2, 2), 2.94 ppm (m, CH_2, 2).

cis,trans-WOSL

Method 1

The second (light pink) band from the chromatography of the original filtrate (see above) was discarded and a third (orange) band collected. This was concentrated and layered with *n*-hexane. Orange crystals were washed with *n*-hexane and dried under vacuum (0.030 g, 10%).

Method 2

A solution of Bu^n_4NSH (0.18 g, 0.69 mmol) in thf:MeCN (10:1, 8 cm^3) was added dropwise to a stirred solution of *cis,trans*-$W^{V}OCIL$ (0.12 g, 0.22 mmol) in thf (10 cm^3). After 3 h, distilled H_2O (50 cm^3) was added aerobically. The orange precipitate was filtered, washed with H_2O and dried in air. It was dissolved in a minimum of CH_2Cl_2 and applied to a silica gel 60 column (mesh 70–230, 10 cm × 2.6 cm diameter) in air. Upon elution with CH_2Cl_2 (4 cm^3 min^{-1}), the first (orange) band was collected, concentrated and layered with *n*-hexane. The thin, dark red sheet crystals were washed with *n*-hexane and dried under vacuum (0.070 g, 60%). Anal. Calcd for $C_{16}H_{18}N_2OS_3W$: C 36.0, H 3.4, N 5.2, S 18.0. Found: C 35.9, H 3.3, N 5.3, S 18.1. EI-MS: *m/z* 534. ^{1}H NMR ($CDCl_3$): 7.30–7.45 (m, Ph, 4 protons), 7.07–7.24 (m, Ph, 4), 4.06 (s, CH_3, 3), 3.58 (s, CH_3, 3), 3.40–3.20 (m, CH_2, 2), 3.09–2.95 ppm (m, CH_2, 2).

cis,cis-WOCIL

A solution of LH_2 (1.24 g, 4.07 mmol) in CH_2Cl_2 (10 cm^3) was added dropwise to a stirred suspension of $(pyH)_2[WOCl_5]$ (1.80 g, 3.35 mmol) in EtOH (50 cm^3). After 1.5 h, the volume was reduced to 30 cm^3 and the red precipitate filtered off, washed with MeOH and dried under a vacuum (1.32 g, 73%). Recrystallisation from a CH_2Cl_2:MeOH (2:1) solution at −16 °C afforded dark red microcrystals which were washed with MeOH and dried under vacuum (36% for recrystallisation step). X-ray quality crystals were grown anaerobically by layering *n*-hexane (2.2 cm^3) onto a solution of *cis,cis*-WOCIL (17 mg) in CH_2Cl_2 (2.5 cm^3). Crystals were isolated after three days at room temperature and dried under vacuum. Anal. Calcd for $C_{16}H_{18}ClN_2OS_2W$: C 35.7, H 3.4, N 5.2. Found: C 35.6, H 3.5, N 5.1. EI-MS: *m/z* 537.

cis,trans-WOCIL

A solution of *cis,cis*-WOCIL (0.20 g, 0.37 mmol) was stirred in air in CH_2Cl_2 (50 cm^3) for 2 h and filtered through Celite to remove a white precipitate. IR spectroscopy indicated that the latter was a mixture of a polyoxotungstate and oxidized ligand. The filtrate was concentrated (5 cm^3) and layered with *n*-hexane (7 cm^3). Dark red crystals were washed with *n*-hexane and dried under vacuum (0.10 g, 52%). Anal. Calcd for $C_{16}H_{18}ClN_2OS_2W$: C 35.7, H 3.4, N 5.2. Found: C 35.5, H 3.2, N 5.1. EI-MS: *m/z* 537. This complex was also obtained by refluxing *cis,cis*-[WOClL] in MeCN overnight and purified by chromatography (silica gel, CH_2Cl_2).

cis,cis-WO(NCS)L

A solution of NaNCS (0.060 g, 0.73 mmol) in EtOH (5 cm^3) was added dropwise to a stirred suspension of *cis,cis*-WOClL (0.38 g, 0.71 mmol) in CH_2Cl_2 (30 cm^3). After 2.5 h, the solution was filtered through Celite, the filtrate reduced to 10 cm^3 and Pr^iOH (5 cm^3) added. After standing at −20 °C for 11 h, the purple microcrystals were filtered off, washed with Pr^iOH and ether and dried under vacuum (0.29 g, 73%). Anal. Calcd for $C_{17}H_{18}N_3OS_3W$: C 36.4, H 3.2, N 7.5. Found: C 36.3, H 3.3, N 7.4. EI-MS: *m/z* 560.

cis,trans-WO(OPh)L

A solution of NaOPh (0.10 g, 0.88 mmol) in thf (8 cm^3) was added dropwise to a stirring suspension of *cis,cis*-WOCIL (0.31 g, 0.58 mmol) in thf (40 cm^3). After 2.5 h, the solvent was removed under vacuum, the residue extracted with a minimum volume of CH_2Cl_2 and the solution applied to a silica gel 60 column (mesh 70–230, 29 cm × 2.3 cm diameter) in air. Upon elution with CH_2Cl_2 (13 $cm^3\ min^{-1}$), the first (pale pink) band was discarded and the second (orange-brown) band collected. Evaporation of solvent yielded an orange-brown amorphous solid (0.17 g, 49%). Anal. Calcd for $C_{22}H_{23}N_2O_2S_2W$: C 4.4, H 3.9, N 4.7. Calcd for $C_{22}H_{23}N_2O_2S_2W.0.33CH_2Cl_2$: C 43.0, H 3.8, N 4.5. Found: C 42.8, H 3.8, N 4.4. EI-MS: *m/z* 595.

cis,trans-WO(SPh)L

A solution of NaSPh (0.17 g, 1.3 mmol) in EtOH (6 cm^3) was added dropwise to a stirred solution of *cis,cis*-WOCIL (0.35 g, 0.64 mmol) in thf (40 cm^3). After 2.5 h, the solvent was removed under vacuum, the residue extracted with CH_2Cl_2 (150 cm^3), the volume reduced to ca. one-third under vacuum and the solution applied to a silica gel 60 column (mesh 70–230, 28 cm × 2.3 cm diameter) in air. Upon elution with CH_2Cl_2 (12 $cm^3\ min^{-1}$), the first (pale yellow) and second (pink) bands were discarded. The third (purple) band was collected. Evaporation of solvent yielded a bright purple amorphous solid (0.13 g, 33%). Anal. Calcd for $C_{22}H_{23}N_2OS_3W$: C 43.2, H 3.8, N 4.6, S 15.7. Found: C 43.1, H 3.9, N 4.5, S 15.6. EI-MS: *m/z* 611.

Physical techniques

Powder infrared spectra were recorded on a Bio-Rad FTS-60A Fourier Transform spectrophotometer using a Digilamp diffuse reflectance accessory in a KBr matrix. EPR spectra of fluid solutions (room temperature) or frozen glasses (77 K) were obtained on a Varian E-line spectrometer incorporating a Varian E-101 microwave bridge using diphenylpicrylhydrazyl ($g = 2.0036$) as reference. UV-visible spectra were recorded on a Hitachi 150–20 spectrophotometer between 800 and 300 nm at a scan rate of 400 nm min^{-1}. Electron impact mass spectrometric measurements were made on a V. G. Micromass 7070F spectrometer operating at 70 eV. The EI-MS values quoted are those of the most intense peak in the parent ion isotope pattern. ^1H and ^{13}C NMR spectra were recorded on Varian Unity 300 (300 MHz) or Bruker Aspect 3000 (300 MHz) Fourier Transform spectrometers using $CHCl_3$ ($\delta = 7.26$) as an internal reference. Electrochemistry was performed using a Cypress CS-1090 Electroanalysis System, Version 6.1/2V and a Cypress CYSY-IR Potentiostat. Solutions, typically 0.5 mM in 0.1 M supporting electrolyte, were prepared anaerobically. Voltammetry at macroelectrodes used a glassy carbon (d = 3 mm) disc working electrode. Voltammetry at microelectrodes used a platinum (23 μ) electrode. The reference electrode consisted of an Ag^+/Ag electrode incorporated into a double salt bridge containing supporting electrolyte to minimise contamination. The auxiliary electrode was a platinum wire. All systems were referenced to SCE using Fc^+/Fc (0.39 V in MeCN, 0.57 V in CH_2Cl_2) as an internal standard [15].

Crystal structure determinations

Single crystals were grown as detailed above. Crystallographic data are given in Table 1, positional parameters in the supplementary material and selected interatomic distances and angles in Table 2. Accurate cell parameters were obtained from least squares refinement of the setting angles of 25 reflections. Intensity data were collected using an Enraf-Nonius CAD-4 MachS single-crystal X-ray diffractometer using Mo$K\alpha$ radiation (graphite crystal monochromator); $\lambda = 0.71073$ Å. The data were corrected for Lorentz and polarisation effects, but a correction for extinction was only applied for *cis,trans*-WOSL. Absorption effects were numerically evaluated by Gaussian integration [19, 20]. All structures were solved using a combination of Patterson map and difference synthesis, using SHELXS-86 [23] and refined using a full-matrix least squares refinement procedure on F, using SHELX-76 [19], apart from *cis,trans*-WOSL, which was refined on F^2, using SHELXL-93 [24]. Anisotropic temperature factors were applied to each of the non-hydrogen atoms. For *cis,cis*-WOClL, *cis,trans*-WOClL and *cis,trans*-WS_2L the atomic scattering factors of the C, H, N, O, S and Cl atoms were those incorporated in the SHELX-76 program system, while the atomic scattering factors for W, and for all the atoms in *cis,trans*-WOSL, were taken from International Tables [21]. Corrections were made for anomalous dispersion [22]. Analyses of variance after the final refinements showed no unusual features. Further details applicable to each of the structures are given below.

cis,trans-WS_2L

Three reflections, monitored after every 9600-s X-ray exposure time, showed no significant variation in intensity. All of the hydrogen atoms, located from the difference map, were constrained at geometrical estimates with a common isotropic temperature factor being assigned to the hydrogens on each methyl carbon and each aromatic ring. Final refinement converged with $R = 0.034$, $R_W = 0.038$, with the maximum peak height in the final difference map being 1.72 e $Å^{-3}$, close to the tungsten atom.

Table 1 Crystallographic data

	cis,cis-WOClL	*cis,trans*-WOClL	*cis,trans*-WOSL	*cis-trans*-WS_2L
Formula	$C_{16}H_{18}ClN_2OS_2W$	$C_{16}H_{18}ClN_2OS_2W$	$C_{16}H_{18}N_2OS_3W$	$C_{16}H_{18}N_2S_4W$
Color	Dark red	Dark red	Red	Dark brown
fw	537.8	537.8	534.4	550.4
Size, mm	$0.12\times0.29\times0.57$	$0.12\times0.37\times0.67$	$0.34\times0.15\times0.10$	$0.38\times0.05\times0.13$
a, Å	13.6541(9)	10.361(3)	10.409(1)	10.645(2)
b, Å	7.1555(11)	14.141(4)	14.205(1)	13.929(2)
c, Å	18.198(2)	12.213(5)	12.092(1)	12.189(2)
β, deg	95.294(6)	102.56(3)	103.07(1)	103.14(2)
V, Å^3	1770.4(3)	1747(2)	1741.6(3)	1760(1)
Z	4	4	4	4
Space group	$P2_1/c$	$P2_1/n$	$P2_1/n$	$P2_1/n$
ρ, g cm^{-3}	2.02	2.05	2.04	2.08
μ, cm^{-1}	68.6	70.9	70.0	69.8
Scan method	$\omega/2\theta$	$\omega/2\theta$	$\omega/2\theta$	$\omega/2\theta$
Data collected	5638	5210	5009	5493
No. of unique data	4049	4010	3989 2892 with $Fo^2>2\sigma(Fo^2)$	4227
$2\theta_{max}$, deg	55	55	55	55
Data refined	3409 [$Fo^2>3\sigma(Fo^2)$]	2748 [$Fo^2>3\sigma(Fo^2)$]	3989	3460 [$Fo^2>2\sigma(Fo^2$]
R[a]	0.039	0.095	0.141	0.034
R_w[b]	0.052	0.117	0.338[c]	0.038
shift/esd	0.00	0.01	0.00	0.00
max diff peak e.Å^{-3}	3.58	1.80	3.56	1.72

[a] $R=\Sigma\|Fo|-|Fc\|/\Sigma|Fo$

[b] $R_w=\Sigma w\|Fo|-|Fc\|^2/\Sigma|Fo|^2$

[c] $R_w=[\Sigma w(Fo^2-Fc^2)^2/\Sigma(Fo^2)^2]^{1/2}$

Table 2 Selected interatomic distances (Å) and angles (°) for *cis,trans*-WS_2L, *cis,trans*WOClL and *cis,cis*-WOClL[a]

	cis,trans-WS_2L	*cis,trans*WOClL	*cis,cis*-WOClL
W-(S4, O)	2.137(1)	1.82(2)	1.691(5)
W-(S3 Cl)	2.146(2)	2.321(8)	2.395(1)
W-N1	2.471(4)	2.23(1)	2.255(5)
W-N2	2.479(4)	2.48(2)	2.461(4)
W-S1	2.382(1)	2.41(1)	2.372(1)
W-S2	2.387(1)	2.40(1)	2.391(2)
(S4, O)-W-(S3, Cl)	105.6(1)	105.1(8)	94.1(2)
(S4, O)-W-N1	93.3(2)	91.4(9)	105.5(2)
(S4, O)-W-N2	162.1(2)	158.3(9)	175.8(2)
(S4, O)-W-S1	103.4(1)	110.1(8)	100.3(2)
(S4, O)-W-S2	89.7(1)	88.2(8)	101.7(2)
N1-W-N2	74.1(2)	74.5(9)	77.6(2)
N1-W-S1	77.0(1)	81.8(8)	81.4(2)
N1-W-S2	83.9(1)	93.6(8)	152.2(2)
S1-W-S2	157.3(1)	161.1(5)	88.1(1)
S2-W-N2	76.7(1)	76.6(6)	75.7(1)
(S3, Cl)-W-N1	159.1(2)	162.8(8)	89.4(2)
(S3, Cl)-W-N2	89.2(2)	90.9(6)	82.9(1)
(S3, Cl)-W-1	89.7(1)	87.9(4)	164.5(1)
(S3, Cl)-W-S2	104.8(1)	91.7(5)	94.5(1)
(S4, O)···C7	3.325(6)	2.95(3)	3.409(9)
(S4, O)···C10	5.433(6)	5.17(3)	4.980(8)
(S4, O)···S1	3.550(2)	3.48(2)	3.150(6)
(S4, O)···S2	3.195(3)	2.96(2)	3.196(6)
(S4, O)···(S3, Cl)	3.410(3)	3.30(2)	3.029(5)
(S3, Cl)···C7	5.452(6)	5.42(3)	3.315(7)
(S3, Cl)···C10	3.276(6)	3.38(2)	3.067(7)
(S3, Cl)···S1	3.197(3)	3.283(12)	4.723(2)
(S3, Cl)···S2	3.593(3)	3.389(13)	3.513(2)

[a] The numbers in parentheses are the estimated standard deviations for the last digit

cis,trans-WOSL

Many crystals of this complex were found to have broad diffraction peaks, indicating that they were disordered. Attempts to obtain better crystals by changing the crystallisation conditions were unsuccessful. The crystal eventually chosen appeared to be the best available, on the basis of peak widths and cell parameters. Three reflections, monitored after every 9600-s X-ray exposure time, showed a 4% decrease in intensity; corrections were applied to the data. After anisotropic refinement of all atoms initially located ($R=0.16$), the resulting difference map showed a peak of height 7.6 e Å^{-3} close to the tungsten atom together with other peaks close to the sulfur and oxygen atoms, which indicated that the structure was disordered in a similar fashion to that observed for *cis,trans*-MoOClL, with some of the molecules in the crystal being rotated by approximately 180 degrees about the *pseudo* twofold axis compared to the others [15]. Both components were included in the refinement, with a refinable site occupation factor assigned. For the minor component, anisotropic temperature factors were able to be assigned only to the W atoms; all other atoms were assigned isotropic temperature factors. During the refinement, all the the C-S distances were constrained to 1.75 Å, while for the minor component the sulphur, oxygen and nitrogen atoms were constrained to have similar geometry to that of the major component. All hydrogen atoms were included for the major component at geometrical estimates; no hydrogens were included for the minor component. Refinement on F^2, using a weighting scheme of the type $[\sigma(Fo^2)+0.0002\ P^2+201.36\ P]^{-1}$, where $P=(Fo^2+2\ Fc^2)/3$, gave final values of $R=0.141$ and $wR=0.338$, where $wR=[\Sigma w(Fo^2-Fc^2)^2/\Sigma(Fo^2)^2]^{1/2}$. An isotropic extinction correction of the form $Fc^*=Fc[1+0.001\ \chi\ Fc^2\ \lambda^3/\sin(2\theta)]^{-1/4}$, where $\chi=0.0032(5)$, was applied to the calculated structure amplitudes. The final occupancy factors for the two components were 0.65(2) and 0.35(2), respectively. During the refinement, the anisotropic temperature factors of several of the carbon atoms were constrained to near isotropic values to prevent them becoming non-positive definite. The final difference map showed several peaks with heights in the range 2.0–3.6 e Å^{-3}, indicating that the disorder was more complicated than described by the model. Attempts to further model this disorder were not successful. The high final R values are a result of this disorder.

cis,cis-WOClL

Three reflections, monitored after every 7200-s X-ray exposure time, showed a 2% decrease in intensity; corrections were made in accordance with this variation. All of the hydrogen atoms were located from the difference map and were constrained at geometrical estimates with a common isotropic temperature factor being assigned to the hydrogens on each methyl carbon and each aromatic ring. Final refinement, with a weighting scheme of type $[\sigma^2(F)+0.0013\ F^2]^{-1}$, gave $R=0.039$ and $R_W=0.052$, with the maximum peak height being 3.58 e Å^{-3}, close to the tungsten atom.

cis,trans-WOClL

Three reflections, monitored after every 9600-s X-ray exposure time, showed a 2% decrease in intensity; corrections were made in accordance with this variation. After anisotropic refinement of all atoms initially located ($R=0.16$), the resulting difference map showed a peak of height 7.9 e Å^{-3} close to the tungsten atom together with other peaks close to the sulfur, oxygen and chlorine atoms, indicating that the structure was disordered in a similar fashion to that observed for the molybdenum analogue [15] and *cis,trans*-WOSL (see above), with some of the molecules in the crystal being rotated by approximately 180 degrees about the *pseudo* twofold axis compared to the others. Both components were included in the refinement, with a refinable site occupation factor assigned. For the minor component, anisotropic temperature factors were able to be assigned only to the W atom, while all other atoms were assigned isotropic temperature factors. During the refinement the atoms of the aromatic rings of the minor component were restrained to ideal geometry, while the other atoms were restrained to have similar geometry to that of the major component. All hydrogen atoms were located for the major component and were fixed at geometrical estimates, but not included in the refinement; no hydrogens were included for the minor component. Final refinement, with a weighting scheme of type $8.129[\sigma^2(F)+0.00015\ F^2]^{-1}$, gave $R=0.095$ and $R_W=0.117$, with the maximum peak height being 1.8 e Å^{-3}, close to the two positions of the disordered tungsten atom. The final occupancy factors for the two components were 0.73(1) and 0.27(1), respectively.

Results

Characterisation of new complexes

cis,trans-$W^{VI}O_2L$ is prepared by direct reaction of *cis*-$WO_2(acac)_2$ and ligand LH_2. B_2S_3 converts it to the $W^{VI}OS$ and $W^{VI}S_2$ analogues but in low yield. The $W^{VI}OS$ compound can be isolated in 60% yield by conversion of *cis,trans*-$W^{V}OClL$ with SH^- to $[W^{V}OSL]^-$ followed by aerial oxidation. *cis,cis*-$W^{V}OClL$ results from direct reaction of $(pyH)_2[W^{V}OCl_5]$ with LH_2. It can be converted to the thermodynamically more stable *cis,trans* species by reflux of an anaerobic solution in MeCN or by stirring a CH_2Cl_2 solution in air. For the latter case, control experiments indicated a requirement for both O_2 and CH_2Cl_2 but not for H_2O. Decomposition occurrs under these conditions in thf or MeCN. Reaction of NaX with *cis,cis*-WOClL provided $W^{V}OXL$. For X = NCS, the *cis,cis* isomer results, while for X = OPh or SPh, the *cis,trans* isomer is obtained.

Parent ions are observed for each complex in electron impact ionisation mass spectra. The experimental mass spectra of *cis,trans*- and *cis,cis*-WOClL were indistinguishable. Characteristic $\nu(W=E)$ (E = O, S) modes are present in infrared spectra of WO_2L, WOSL and WS_2L (Table 3). The infrared spectra of WOXL are very similar to those of the analogous molybdenum compounds [15], indicating that the spectroscopic differences associated with ligand conformation are maintained in the tungsten system. In particular, the relative intensities of the absorptions at approximately 895 and 845 cm^{-1} are an indicator of ligand stereochemistry in WOXL complexes (Table 3). Electronic spectra are qualitatively similar to the molybdenum analogues [15], but the lowest energy absorption is blue shifted (Table 4). Again, stereochemical assignment is possible: the *cis,cis* isomers show a prominent shoulder on the latter band.

^{1}H NMR data (see Experimental section) are consistent with effective C_2 point symmetry for $W^{VI}E_2L$ (E = O, S), confirming the presence of the *cis,trans* isomers in solution. The spectrum of WOSL indicates C_1 point symmetry, consistent with either the *cis,trans* or *cis,cis* isomer. Intense absorptions characteristic of thio- or thiolate-to-metal charge transfer transitions are present in electronic spectra (Table 4).

Table 3 Infra-red maxima (cm^{-1})

Complex	Isomer	ν(W=O)	ν(W=S)	Intensity at 895>845 cm^{-1}?[a]	
WO_2L	*cis,trans*	943, 903			
WOSL	*cis,trans*	928	492		
WS_2L	*cis,trans*		499, 487		
WO(NCS)L	*cis,cis*	957, 947		2034 (NCS)	Yes
WOClL	*cis,cis*	960, 948			Yes
WOClL	*cis,trans*	964			No
WO(OPh)L	*cis,trans*	947		1239 (CO) 638 (WO)	No
WO(SPh)L	*cis,trans*	939		No	

[a] Criterion of stereochemistry (see text)

Table 4 Electronic spectra (nm)

Complex	Isomer	Solvent	λ_{max} (log)
WO_2L	*cis,trans*	MeCN	334 (3.76), 368 sh
WOSL	*cis,trans*	CH_2Cl_2	341 (3.61), 447 (3.59)
WS_2L	*cis,trans*	CH_2Cl_2	377 (3.71), 4.10 sh, 444 (3.74)
WO(NCS)L	*cis,cis*	MeCN	370 (3.67), 495 (3.53), 570 sh
WOClL	*cis,cis*	MeCN	332 (3.57), 390 sh, 476 (3.36), 553 (3.13)
WOClL	*cis,trans*	MeCN	317 (3.54), 353 sh, 380 sh, 513 (3.54)
WO(OPh)L	*cis,trans*	CH_2Cl_2	380 (3.56), 479 (3.57)
WO(SPh)L	*cis,trans*	CH_2Cl_2	318 sh, 378 (3.58), 544 (3.62)

Molecular structures

X-ray crystallography confirms the presence of the *cis,trans* isomer in WS_2L (Fig. 2), isostructural with *cis,trans*-$Mo^{VI}O_2L$ [14]. The average W=S bond distance of 2.14 Å (Table 2) lies within the 2.06–2.18 Å range observed for such links and is very close to those observed in *cis*-$WS_2(OPh)(L\text{-}N_3)$ and (η^5-C_5Me_5)$WS_2(CH_2SiMe_3)$ [11, 25]. The *trans* influence of the thio ligands imposes relatively long W-N distances of 2.47 and 2.48 Å. Non-bonded interactions determine the detailed coordination geometry, as seen in related systems [15]. In particular, differential interactions between thio ligand S3 and the two $N(Me)C_6H_4S$ chelate fragments provide two distinct S3-W-S1,2 angles (89.7, 104.8°) and S3···S1,2 distances(3.20, 3.59 Å). The smaller angle and distance occurs when the W-S3 vector is parallel to the chelate plane and the larger when it is perpendicular (Fig. 2). Equivalent geometry is seen around thio ligand S4 (Table 2).

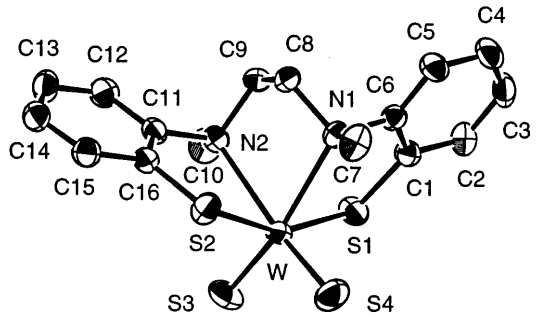

Fig. 2 Molecular structure of *cis,trans*-WS_2L with 50% probability displacement. Hydrogen atoms are omitted

The structure of WOSL is disordered, with some of the molecules in the crystal rotated by approximately 180° about the *pseudo* twofold axis compared to the others. The derived structure is of low quality but does confirm the stoichiometry and the presence of the *cis,trans* isomer.

The molecular structure of *cis,cis*-WOClL is isostructural with its molybdenum analogue (Fig. 3a) [15]. It features a short Cl···C10 distance, 3.07 Å, and acute O-W-Cl bond angle, 94° (Table 2), symptomatic of the steric crowding characteristic of this stereochemistry [15]. Conversion to the more stable *cis,trans* isomer changes these parameters to 3.38 Å and 105°, respectively (Fig. 3b, Table 2).

Electrochemistry

Cyclic voltammograms of *cis,trans*-$W^{V}O(OPh)L$ at a glassy carbon electrode (d=3 mm) in MeCN (0.13 M Bu_4NBF_4) reveal an oxidation at 230 mV vs SCE and a reduction at −1250 mV (Fig. 4). Quantitative data are consistent with each process being a reversible, one-electron event (Table 5) [26]. Steady-state voltammograms at a platinum micro-electrode (d=23 μ) support this conclusion: plots of E versus $\ln(i_L - i)/i$ are linear, the slopes providing estimates of 1.1 for the number of electrons, n, transferred in the processes (X=OPh; Table 5) [27, 28][1].

$$[W^{VI}OXL]^+ + e^- = W^{V}OXL \quad (1)$$

$$W^{V}OXL + e^- = [W^{IV}OXL]^- \quad (2)$$

[1] For reduction of *cis,trans*-$W^{V}O(OPh)L$ (X=OPh, SPh) and -WS_2L, steady state voltammograms at v=10 mVs^{-1} showed an oxidative return wave which did not closely retrace the reductive wave, suggesting irreversibility. These observations are similar to those seen in the molybdenum systems [15]. At higher scan rates (20–50 mVs^{-1}), the behaviour was that expected for a reversible process. A likely explanation is interference due to absorption of products to the electrode surface at the slow scan rate of 10 mVs^{-1} employed to ensure steady state conditions

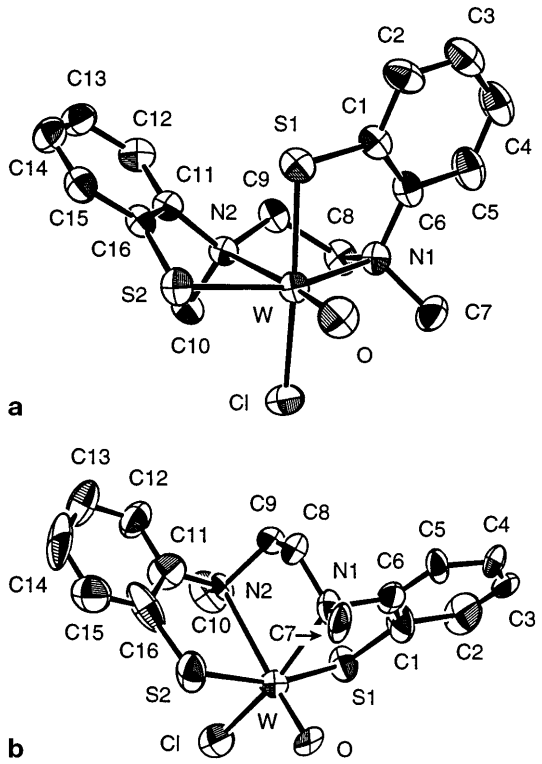

Fig. 3 Molecular structure of **a** *cis,cis*-WOClL and **b** *cis, trans*-WOClL with 50% probability displacement. Hydrogen atoms are omitted

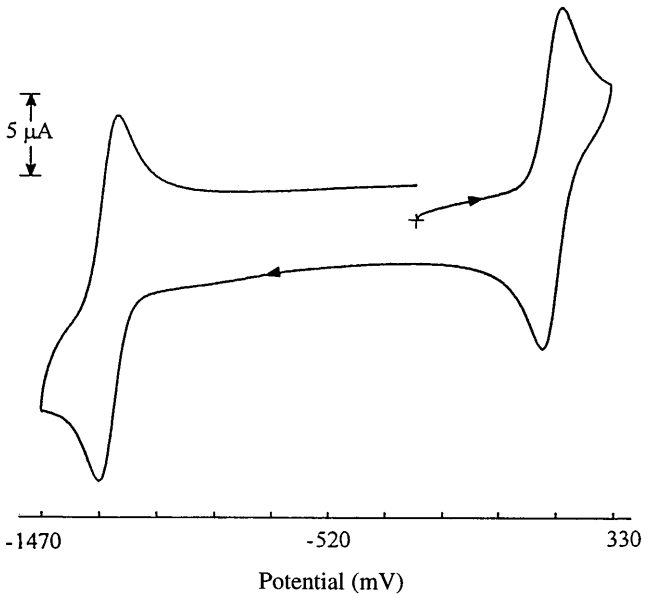

Fig. 4 Cyclic voltammogram of *cis,trans*-WO(OPh)L in MeCN (0.5 mM, 0.13 M Bu_4NBF_4, 21 °C, 100 mV s^{-1})

Similar results are seen for the other *cis,trans* compounds, X = SPh, Cl (Table 6). For *cis,cis*-WOClL with Bu_4NBF_4 as electrolyte, a quasi-reversible [26] oxidation is observed at 615 mV and an irreversible reduction process at −930 mV with an associated reoxidation centred around 380 mV. With Et_4NCl as electrolyte, both primary processes are irreversible.

Complexes *cis,trans*-WO_2L, -WOSL and -WS_2L[1] in MeCN or CH_2Cl_2 (0.1 M Bu_4NBF_4) exhibit single reduction events as their only observable redox process. Quantitative data are consistent with reversible, one-electron couples (Table 6); for example:

$$W^{VI}O_2L + e^- = [W^{V}O_2L]^- \quad (3)$$

Electron Paramagnetic Resonance

Table 7 lists spectral parameters for each complex $W^{V}OXL$ ($5d^1$). Each anisotropic component consists of a central resonance from molecules containing even isotopes of tungsten ($I = 0$, 85.6 atom%) flanked by two hyperfine lines from molecules containing odd isotopes ($I = 1/2$, 14.4 atom%). Linewidths are usually broader

Table 5 Cyclic voltammetric data for *cis,trans*-WO(OPh)L[a]

v, mV s^{-1}	E_{pa}, mV	E_{pc}, mV	ΔE_p, mV	$E_{1/2}$, mV	i_{pa}, mA M^{-1}	i_{pc}, mA M^{-1}	i_{pa}/i_{pc}	$i_{pc}\,v^{-1/2}$, mA $s^{1/2}$ $mV^{-1/2}$
				Couple 1				
20	265	200	65	233	5.5	5.6	1.0	40
50	260	200	60	230	9.0	9.3	1.0	42
100	260	200	60	230	12.7	13.0	1.0	41
200	265	200	65	230	15.9	16.4	1.0	37
500	265	195	70	230	25.8	26.6	1.0	38
1000	265	195	70	230	37.7	38.5	1.0	39
				Couple 2				
20	−1215	−1275	60	−1245	6.6	6.0	1.1	42
50	−1220	−1280	60	−1250	10.0	9.0	1.1	40
100	−1220	−1280	60	−1250	13.7	12.8	1.1	41
200	−1215	−1285	70	−1250	18.4	16.8	1.1	38
500	−1210	−1285	75	1245	28.7	27.5	1.0	39
1000	−1210	−1290	80	−1250	41.3	39.1	1.1	39

[a] 0.46 mM, 0.13 M Bu_4NBF_4, MeCN, 16 °C, glassy carbon electrode (d = 3 mm). Potentials versus SCE using ferrocene as an internal standard

Table 6 Electrochemical data[a,b]

Complex	Isomer	Solvent (electrolyte[c])	Reversibility	$E_{1/2}$[d] or E_p[e], mV	ΔE_p[e] mV	i_{pa}/i_{pc}	n[f]
WO_2L	*cis,trans*	MeCN (BF_4^-)	Rev	−1505	67	1.1	1.0
WOSL	*cis,trans*		Rev	−1090	69	1.1	1.1
WOSL	*cis,trans*	CH_2Cl_2 (BF_4^-)	Rev	− 970	89	1.0	1.0
WS_2L	*cis,trans*		Rev	− 970	81	1.0	1.1
WO(NCS)L	*cis,cis*	MeCN (BF_4^-)	Q-rev	630	69	1.4	1.1
			Q-rev	− 775	65	0.9	1.1
WOClL	*cis,cis*		Q-rev	615	61	1.2	1.1
			Irrev	− 930			
		MeCN (Cl^-)	Irrev	465			
			Irrev	− 900			
WOClL	*cis,trans*	MeCN (BF_4^-)	Q-rev	630	61	1.0	1.1
			Rev	−1015	62	1.1	1.0
		MeCN (Cl^-)	Irrev	610			
			Rev	− 995	65	1.1	1.0
WO(OPh)L	*cis,trans*	MeCN (BF_4^-)	Rev	230	59	1.0	1.1
			Rev	−1250	60	1.1	1.1
WO(SPh)L	*cis,trans*	MeCN (BF_4^-)	Q-rev	505	67	1.6	1.2
			Rev	− 895	65	1.0	1.2
	cis,trans	CH_2Cl_2 (BF_4^-)	Rev	615	73	1.1	1.3
			Rev	− 785	72	1.0	1.0

[a] Potentials versus SCE using ferrocene as an internal standard
[b] 0.4–0.6 mM
[c] 0.12–0.13 M, Bu_4N^+ salt
[d] Estimated from cyclic voltammetry at a glassy carbon electrode (dia = 3 mm) or steady state voltammetry at a platinum micro-electrode (dia = 23 μ). Quoted for rev or q-rev processes only
[e] Observed by cyclic voltammetry (v = 100 m Vs^{-1}). E_p quoted for irrev processes
[f] Estimated from the slope of the graph E versus $\ln(i_l - i)/i$ derived from steady state voltammetry

Table 7 EPR parameters[a]

Species[a]	g				A(^{183}W), 10^{-4} cm^{-1}				A(^{1}H), 10^{-4} cm^{-1}				Ref.
	1	2	3	av	1	2	3	av	1	2	3	av	
cis,cis-WO(NCS)L[b]	1.949	1.856	1.837	1.88	94			66					
cis,cis-WOClL[b]	1.951	1.842	1.822	1.87	94	57	60	70					
cis,trans-WOClL[b]	1.933	1.833	1.808	1.85	96	69	60	75					
cis,trans-WO(OPh)L[b]	1.903	1.824	1.803	1.83	88	58	85	80					
cis,trans-WO(SPh)[b]	2.006	1.864	1.855	1.90	84	41	53	60					
$[WO(SPh)_4]^-$	2.018	1.903	1.903	1.936	78.1	44.4	44.4	55.1					18
$[WO(bdt)_2]^-$	2.044	1.931	1.911	1.962	78	40	37	52					44
$[WO(edt)_2]^-$	2.105	1.919	1.894	1.973									45
$[WO(SePh)_4]^-$	2.086	1.923	1.923	1.971	74.0	43.3	43.3	50.6					18
cis,trans-$[WO_2L]^-$[c]	1.859	1.707	1.509	1.70									
cis,trans-WO(OH)L[c]	1.892	1.804	1.804	1.83	87				16				
cis,trans-$[WOSL]^-$[c]	1.953	1.770	1.690	1.79	75			~67					
cis,trans-WO(SH)L[c]	1.999	1.857	1.844	1.90	86	ca. 40			11	16	ca. 15	ca. 14	
Aldehyde oxido-Reductase (active)[d]	1.989	1.901	1.863	1.918	52	27	46	42					2, 39
Sulfite oxidase[e]													40
(low pH)	1.98	1.89	1.87	1.91	81	~41	~41	~54	~7				
(high pH)	1.93	1.87	1.84	1.88									
Formylmethanofuran Dehydrogenase[f]	2.049	2.012	1.964	2.008	48	43	28	40					41
Formate dehydrogenase[g]	2.101	1.980	1.950	2.010									42

[a] Estimated directly from the spectra for the synthetic species reported here
[b] Spectra measured in 25:1 thf:MeCN, 0.10 M $(Bu_4^n)BF_4$. W conc. about 5 mM
[c] Generated in 25:1 thf:MeCN, 0.05 mM $(Bu_4^n)SH$
[d] Low potential, active form (poised at −450 mV versus standard hydrogen electrode) from *Pyrococcus furiosus*
[e] Tungsten-substituted molybdenum enzyme from tungsten-treated rats, sulfite-reduced, parameters estimated from published spectra
[f] Tungsten-substituted molybdenum enzyme from *Methanobacterium wolfei* in air
[g] From *Clostridium thermoaceticum* (poised at −450 mV versus standard hydrogen electrode)

than for molybdenum analogues due to greater anisotropy of the **g** and **A** matrices [17, 29]. Spectra of the *cis,cis* and *cis,trans* forms of WOClL are shown in Fig. 5.

WO_2L in MeCN (0.1 M Bu_4NBF_4) was reduced by controlled potential electrolysis at −1.5 V (Table 6). The solution was transferred rapidly by cannula to an EPR sample tube and frozen immediately. A highly anisotropic signal was observed and assigned to $[W^{V}O_2L]^-$ (Table 7) by analogy with the corresponding molybdenum system [14, 30]. When reduced in the presence of H_2O (1.5 M), the spectrum exhibited diminished anisotropy and the features occurred as doublets. Generation in the presence of ^2H_2O caused the doublets to collapse, indicating that the superhyperfine structure arises from coupling to a single proton. The signal is assigned to $W^{V}O(OH)L$. Reaction of Bu_4NSH with *cis,trans*-$W^{V}OClL$ or -$W^{VI}OSL$ in thf:MeCN (25:1, 0.1 M Bu_4NBF_4) results in a broad EPR signal ($g=1.787$) in mobile solution, assignable to $[W^{V}OSL]^-$. Its frozen solution spectrum is shown in Fig. 6a. Reaction with *cis,cis*-$W^{V}OClL$ also generates this signal, but its much lower intensity suggests that EPR-silent species are also formed. Addition of two equivalents of CF_3CO_2H to $[W^{V}OSL]^-$ at −100 °C gave a red solution which, when frozen, exhibits a spectrum with doublets on all three components (Fig. 6b). The signal is assigned to $W^{V}O(SH)L$. This signal is replaced by a new one ($g=1.904$) upon warming. The new signal has no resolved proton coupling and may also be generated by reaction of *cis,cis*-$W^{V}OClL$ with four equivalents of SH^- at room temperature. The nature of the species responsible is not known. Similar behaviour obtains for the equivalent molybdenum system [14]. Although WOSL and WS_2L have similar reduction potentials (Table 6), attempted reduction of the latter with SH^- failed to generate EPR-active species.

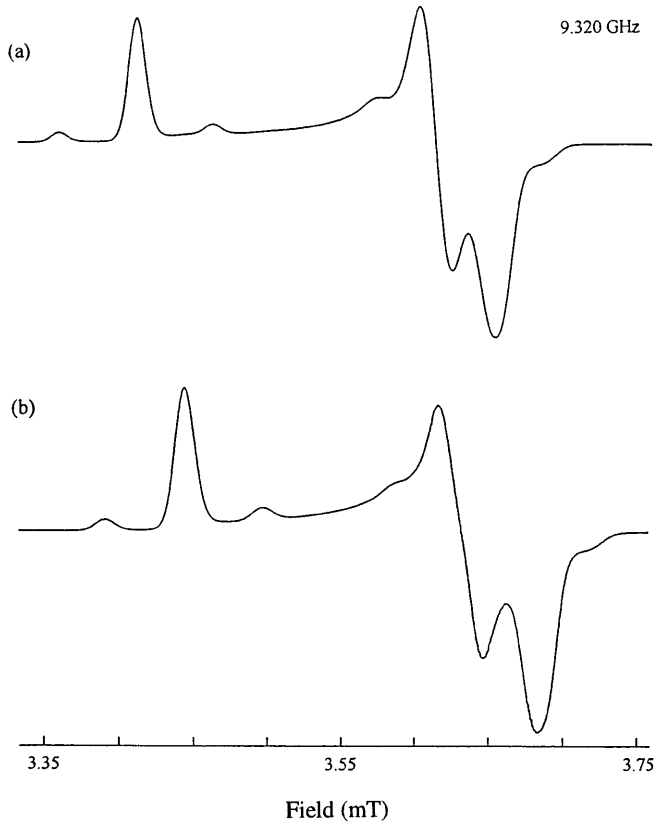

Fig. 5 EPR spectra of WOClL in thf:MeCN mixture (10:1; 0.1 M Bu_4NBF_4), 77 K: **a** *cis,cis*; **b** *cis,trans*

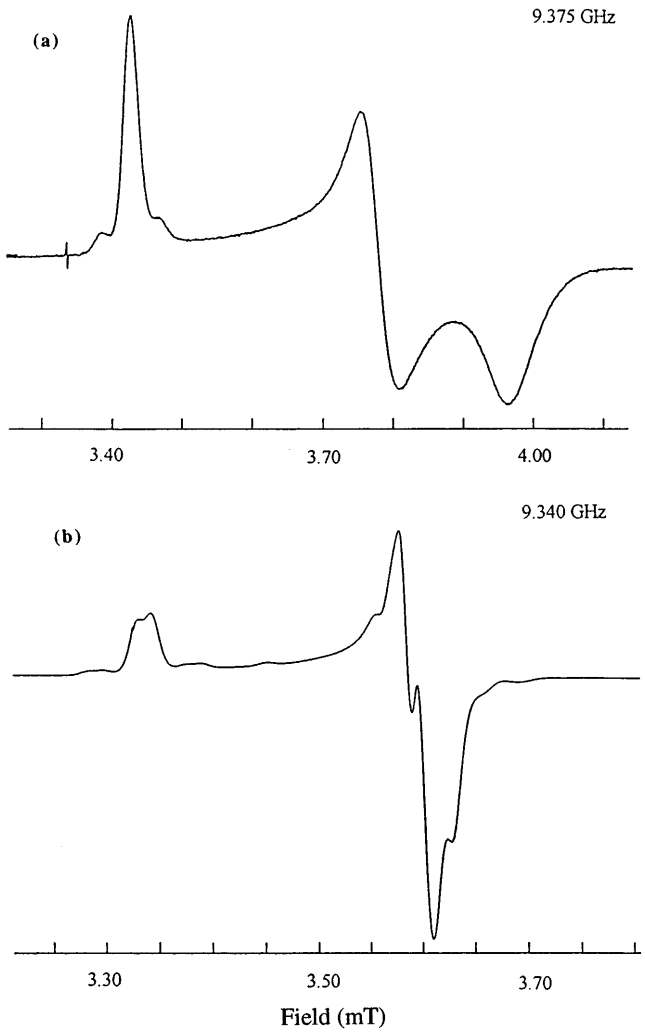

Fig. 6 EPR spectra in thf:MeCN (10:1, 0.1 M Bu_4NBF_4), 77 K: **a** $[W^{V}OSL]^-$; **b** $W^{V}O(SH)L$

Discussion

The properties of the complexes *cis,trans*-$W^{VI}O_2L$, -$W^{VI}OSL$, -$W^{VI}S_2L$ and -$W^{V}OXL$ (X=Cl, OPh, SPh) and of *cis,cis*-$W^{V}OXL$ (X=Cl, NCS) isolated in the present work can be compared with the molybdenum analogues $Mo^{VI}O_2L$ and $Mo^{V}OXL$ [14, 15]. The stereochemistry of quadridentate ligand L observed in complexes $Mo^{V}OXL$ depends upon the steric proper-

ties of anionic ligand X. A *cis*-S,S conformation leads to a short $H_3C\cdots X$ distance and an acute O-W-X bond angle, which destabilizes that arrangement relative to the *trans*-S,S conformation. The *cis,cis* isomers have not been observed for sterically demanding ligands X such as OPh and SPh. For the $M^{VI}E_2L$ complexes, the *cis,trans* isomer only has been isolated in substance. The *cis,cis* isomer imposes an anionic thiolate ligand *trans* to oxo or thio (see Fig. 3) which is disfavored by the strong π-donor properties of those ligands in M(VI) species. In addition, an acute EME bond angle between *cis* M=E (E=O or S) functions is destabilized by repulsion between the multiple bonds.

As expected, the tungsten complexes $W^{V}OXL$ are more difficult to reduce than their molybdenum analogues [15, 31]. Shifts of 270–450 mV are observed. The reversible behaviour of the three *cis,trans* complexes (X=Cl, OPh, SPh) highlights the relative stability of that stereochemistry relative to *cis,cis* and the simpler behavior of these tungsten complexes relative to the molybdenum analogues. Access to W(VI) and W(IV) species from a W(V) complex (Eqs. 1, 2, Fig. 4) has been observed previously only in certain hindered $[W^{V}O(SR)_4]^-$ systems [32].

In the presence of excess chloride, *cis,cis*-MoOClL and -WOClL exhibit different electrochemistries (Table 6). One-electron reduction of the former is reversible in excess chloride but irreversible in its absence. This was attributed to the presence of a rapid equilibrium between $[Mo^{IV}OClL]^-$ and $Mo^{IV}OL$ [15]. Under the same conditions, reduction of WOClL remains irreversible, suggesting that the equivalent equilibrium more strongly favours dissociation of chloride ligand.

Each of the complexes *cis,trans*-$W^{VI}O_2L$, -$W^{VI}OSL$ and -$W^{VI}S_2L$ exhibits a reversible W^{VI}/W^{V} couple (e.g. Eq. 3). This highlights the ability of ligand L to sterically inhibit the chemical changes which normally follow reduction of $M^{VI}O_2$ (M=Mo, W) and related centres [14]. The $E_{1/2}$ value for WO_2L is about 500 mV more negative than that of MoO_2L [15] and 400 mV more negative than that of WOSL (Table 6), respectively. Similar properties hold for $M^{VI}O_2Cl(L\text{-}N_3)$ and $M^{VI}OSCl(L\text{-}N_3)$ [11, 33]. It is apparent that substitution of terminal thio for oxo at $W^{VI}O_2$ centers causes $E_{1/2}$ values to fall into the range observed for $Mo^{VI}O_2$ species and so to become biologically accessible. The $E_{1/2}$ value of WS_2L is very similar to that of WOSL (Table 6). This observation is contrary to the progressive positive shifts observed in the *pseudo*-tetrahedral hydroxylamido complexes $Mo^{VI}E_2(C_5H_{10}NO)_2$ ($E_2=O_2$, OS, S_2) [34]. This feature is not understood but may be related to the sulfur-rich environment of WS_2L.

Isolation in substance of $W^{VI}OSL$ and $W^{VI}S_2L$ and of similar species with ligand $L\text{-}N_3$ [10, 11] contrasts with the instability of the six-coordinate molybdenum analogues. The only stable molybdenum species of this type isolated to date, $MoOS(S_2PPr^{i}_2)(L\text{-}N_3)$ and $MoO(S_2py)(L\text{-}N_3)$, feature steric or redox "protection" [35, 36].

The well-behaved redox properties of the W(VI) species allow generation of reduced forms $[W^{V}O_2L]^-$ and $[W^{V}OSL]^-$ and their conjugate acids $W^{V}O(OH)L$ and $W^{V}O(SH)L$. Characterisation of the equivalent molybdenum species in solution assisted assignment of the centres responsible for the characteristic EPR signals of molydo-enzyme species [14, 30, 37–39]. EPR data for tungsten centres in enzymes are just becoming available (Table 7) [1, 40–43]. A full listing is given in [2]. The broader linewidths of W spectra compared to Mo spectra make it difficult to resolve hyperfine couplings in 1D spectra. The EPR parameters derived in the present study (Table 7) have been estimated directly from the spectra, and so there is uncertainty about the influence of non-coincidence of **g** and **A** tensor axes.

$[W^{V}O_2L]^-$ and $[W^{V}OSL]^-$ exhibit g_3 parameters below 1.7, which leads to g_{av} values below 1.8. As such features are not apparent in any of the enzyme spectra [1], $W^{V}O_2$ and $W^{V}OSL$ centres are unlikely to be present in the known systems.

Mirroring a similar trend for oxo-molybdenum(V) centers [44], there is some evidence for a correlation between g_{av} and the number of thiolate ligands in oxotungsten(V) species: 1.83 {WO(OH)L, WO(OPh)L}, 1.90 {WO(SH)L, WO(SPh)L}, 1.94 {$[WO(SPh)_4]^-$}. A_{av} would appear to decrease in the same order (Table 7). A comparison with the parameters of active aldehyde oxidoreductase from *P. furiosus* provides some support for the current working model of a $W^{V}O(OH)(S)_{3-4}$ site [1]. It is important not to over-interpret the present preliminary data available for the enzyme and synthetic species. For example, a simple comparison of g, $A(^{183}W)$ and $A(^{1}H)$ parameters of tungsten-substituted molybdenum sulfite oxidase (low pH) and $W^{V}O(OH)L$ suggest that a $W^{V}O(OH)$ center is responsible for the enzyme spectrum. This correlates with the assignment of a $Mo^{V}O(OH)$ centre to the equivalent native enzyme spectrum [2]. However, the parameters observed for WO(OH)L, for active aldehyde oxidoreductase and for sulfite oxidase indicate that the influence of the other ligands on a putative $W^{V}O(OH)$ centre is important. There is a particular need for bis(1,2-dithiolato)tungsten centres without oxo groups, given the apparent importance of centres such as $Mo^{VI}(OH)(Se\text{-}Cys)(S)_4$ in molybdenum formate dehydrogenase [9]. The high g values observed for tungsten formate dehydrogenase and formylmethanofuran dehydrogenase (Table 7) are consistent with $W^{V}(OH)(Y\text{-}Cys)(S)_{3-4}$ (Y=S, Se) in those systems [1, 42].

Acknowledgements K. B. acknowledges the award of an APRA postgradute scholarship. A.G.W. thanks the Australian Research Council for financial support (Grant no. 290 30599). Prof. J. T. Spence and Mr. R. J. Greenwood are thanked for preliminary EPR measurements.

References

1. Johnson MK, Rees DC, Adams MWW (1996) Chem Rev 96:2817–2839
2. Hille R (1996) Chem Rev 96:2757–2816
3. Young CG, Wedd AG (1997) J Chem Soc, Chem Commun, 1251–1257
4. Eagle AE, Thomas S, Young CG. In: Transition Metal Sulfur Chemistry; Stiefel EI, Matsumoto K, Eds. ACS Symposium Series 653; American Chemical Society: Washington, DC, 1996, pp 324–335
5. Mukund S, Adams MWW (1991) J Biol Chem 266:14208–14216
6. Chan MK, Makund W, Kletzin A, Adams MWW, Rees DC (1995) Science 267:1463–1469
7. George GN, Prince RC, Mukund S, Adams MWW (1992) J Am Chem Soc 114:3521–3523
8. Cramer SP, Liu C-L, Mortenson LE, Spence JT, Liu S-M, Yamamoto I, Ljungdahl LG (1985) J Inorg Biochem 23:119–124
9. Boyington JC, Gladyshev VN, Khangulov SV, Stadtman TC, Sun PD (1997) Science 275:1305–1308
10. Eagle AA, Tiekink ERT, Young CG (1991) J Chem Soc, Chem Commun 1746–1748
11. Eagle AA, Harben SM. Tiekink ERT, Young CG (1994) J Am Chem Soc 116:9749–9750
12. Ueyama N, Oku H, Nakamura A (1992) J Am Chem Soc 114:7310–7311
13. Das SK, Biswas D, Maiti R, Sarkar S (1996) J Am Chem Soc 118:1387–1397
14. Dowerah D, Spence JT, Singh R, Wedd AG, Wilson GL, Farchione F, Enemark JH, Kristofzski J, Bruck MJ (1987) J Am Chem Soc 109:5655–5665
15. Barnard KR, Bruck M, Huber S, Grittini C, Enemark JH, Gable RW, Wedd AG (1997) Inorg Chem 36:637–649
16. Yu S, Holm RH (1989) Inorg Chem 28:4385–4391
17. Hanson GR, Brunette AA, McDonell AC, Murray KS, Wedd AG (1981) J Am Chem Soc 103:1953–1959
18. Kornblum N, Lurie AP (1959) J Am Chem Soc 81:2705–2715
19. Sheldrick GM. SHELX-76, Program for Crystal Structure Determination; University of Cambridge: Cambridge UK, 1976
20. International tables for X-ray crystallography (1992) Kluwer Academic, Dordrecht, The Netherlands, vol C, p 200
21. International tables for X-ray crystallography (1992) Kluwer Academic, Dordrecht, The Netherlands, vol C, p 500
22. International tables for X-ray crystallography (1992) Kluwer Academic, Dordrecht, The Netherlands, vol IV, p 219
23. Sheldrick GM. SHELXS-86, Program for Crystal Structure Solution, Acta Cryst., 1990, A46 467
24. Sheldrick GM. SHELXL-93, Program for the Refinement of Crystal Structures University of Gottingen, Germany, 1993
25. Faller JW, Kucharczyk RR, Ma Y (1990) Inorg Chem 29:1662–1667
26. Bard AJ, Faulkner LR Eds (1980) Electrochemical Methods: Fundamentals and Applications; Wiley: New York, Chapter 4
27. Montenegro MI, Queirós MA, Daschbach JL, Eds. (1991) Microelectrodes: Theory and Applications; Kluwer Academic: Dordrecht
28. Bond AM, Oldham KB, Zoski CG (1989) Anal Chim Acta 216:177–230
29. Hanson GR, Wilson GL, Bailey T D, Pilbrow JR, Wedd AG (1987) J Am Chem Soc 109:2609–2616
30. Greenwood RJ, Wilson GJ, Pilbrow JR, Wedd AG (1993) J Am Chem Soc 115:5385–5392
31. Rice CA, Kroneck PMH, Spence JT (1981) Inorg Chem 20:1996–2000
32. Soong S-L, Chebolu V, Koch SA, O'Sullivan T, Millar M (1986) Inorg Chem 25:4067–4068
33. Roberts SA, Young CG, Kipke CA, Cleland WE Jr, Yamanouchi K, Carducci MD, Enemark JH (1990) Inorg Chem 29:3650–3656
34. Traill PR, Bond AM, Wedd AG (1994) Inorg Chem 33:5754–5760
35. Eagle AA, Laughlin LJ, Young CG, Tiekink ERT (1992) J Am Chem Soc 114:9195–9196
36. Hill JP, Laughlin LJ, Gable RW, Young CG (1996) Inorg Chem 35:3447–3448
37. Wilson GL, Greenwood RJ, Pilbrow JR, Spence JT, Wedd AG (1991) J Am Chem Soc 113:6803–6812
38. Greenwood RJ, Wilson GL, Pilbrow JR, Wedd AG (1993) J Am Chem Soc 115:5385–5392
39. Xiao Z, Gable RW, Wedd AG, Young CG (1996) J Am Chem Soc 118:2912–2921
40. Koehler BP, Mukund S, Conover RC, Dhawan IK, Roy R, Adams MWW, Johnson MK, submitted for publication
41. Johnson JL, Rajagopalan KV (1976) J Biol Chem 251:5505–5511
42. Schmitz RA, Albracht SPJ, Thauer RK (1992) FEBS Lett 309:78–81
43. Deaton JC, Solomon EI, Watt GD, Wetherbee PJ, Durfor CN (1987) Biochem Biophys Res Commun 149:424–430
44. Dhawan IK, Enemark JH (1996) Inorg Chem 35:4873–4882
45. Oku H, Ueyama N, Nakamura A (1995) Chem Lett 621–622
46. Ellis SR, Collison D, Garner CD, Clegg WJ (1986) Chem Soc, Chem Commun 1483–1485